Linear stability of layered two-phase flows through parallel soft-gel-coated walls

B. Dinesh and S. Pushpavanam*

Department of Chemical Engineering, Indian Institute of Technology Madras, Chennai 600 036, India

(Received 7 April 2017; published 31 July 2017)

The linear stability of layered two-phase Poiseuille flows through soft-gel-coated parallel walls is studied in this work. The focus is on determining the effect of the elastohydrodynamic coupling between the fluids and the soft-gel layers on the different instabilities observed in flows between parallel plates. The fluids are assumed Newtonian and incompressible, while the soft gels are modeled as linear viscoelastic solids. A long-wave asymptotic analysis is used to obtain an analytical expression for the growth rate of the disturbances. A Chebyshev collocation method is used to numerically solve the general linearized equations. Three distinct instability modes are identified in the flow: (a) a liquid-liquid long-wave mode; (b) a liquid-liquid short-wave mode; (c) a gel-liquid short-wave mode. The effect of deformability of the soft gels on these three modes is analyzed. From the long-wave analysis of the liquid-liquid mode a stability map is obtained, in which four different regions are clearly demarcated. It is shown that introducing a gel layer near the more viscous fluid has a predominantly *stabilizing* effect on this mode seen in flows between rigid plates. For parameters where this mode is stable for flow between rigid plates, introducing a gel layer near the less viscous and thinner fluid has a predominantly *destabilizing* effect. The liquid-liquid short-wave mode is *destabilized* by the introduction of soft-gel layers. Additional instability modes at the gel-liquid interfaces induced by the deformability of the soft-gel layers are identified. We show that these can be controlled by varying the thickness of the gel layers. Insights into the physical mechanism driving different instabilities are obtained using an energy budget analysis.

DOI: 10.1103/PhysRevE.96.013119

I. INTRODUCTION

Layered flows through channels lined with soft deformable gels are encountered in a wide variety of microfluidic applications [1]. Soft materials are often used in fabrication of microchannels [2,3]. An understanding of the physics behind the interaction between the walls of the soft gel and the two-phase flow past the gel will help in accurate design and development of lab on chip applications. There has been extensive experimental and theoretical work focusing on stability of two-phase flows through rigid channels. Two-phase layered flows are unstable to a viscosity induced long-wave interfacial instability [4]. Energy transfer from the base state to perturbed flow can arise due to density stratification, shape of velocity profile, viscosity stratification, shear effects, and a combination of viscosity and shear effects in these flows. A long-wave interfacial instability was first identified by Yih [5]. For higher Reynolds numbers a shear instability was observed as reported in [6]. This Tollmien-Schlichting mode was primarily caused by shear stresses generated near the walls. The study of two-phase layered flows between rigid channels reported in [6] was extended by the authors of [7] to study the effect of channel height and thickness of the fluids. Instabilities arising due to viscosity stratification are discussed in [8]. Interfacial instabilities in two-phase layered flows were experimentally studied in [9–12].

The dynamics of fluid flow past a deformable soft gel is different from that of the fluid flow past a rigid surface due to the elastohydrodynamic coupling between the soft gel and the fluid. This coupling gave rise to instabilities in single-phase Couette flow over a linear viscoelastic gel layer in the creeping flow limit [13]. It was shown that the instability arose from the work done by the mean flow at the interface which resulted in energy transfer from the mean flow to the fluctuations. The stability of a pressure driven flow in a circular pipe lined by a linear viscoelastic material was studied [14]. Here the gel-liquid interface becomes unstable when the gel was sufficiently deformable in the creeping flow limit. Stability of pressure driven flows through cylindrical tubes lined with a linear viscoelastic material for intermediate Reynolds number was studied [15,16]. It was shown that the transition from laminar to turbulent flow in a gel lined tube occurs at a much lower Reynolds number than in a rigid-walled tube. Linear stability of flow through a flexible pipe and Couette flow over a flexible gel were studied [17]. The different instabilities were classified into three significant modes depending on the underlying cause: viscous modes, wall modes, and inviscid modes. A neo-Hookean solid model was used to study linear stability of different flow systems [18–21,22]. It was shown that a first normal stress difference in the base state leads to an instability that is different from that observed in linear viscoelastic solids.

Linear stability of a two-layer plane Couette flow of a Maxwell fluid past a linear viscoelastic solid was studied [21]. It was shown that the effect of the gel on the stability of the two-fluid interface depends on the viscosity ratio of the fluids. Linear stability of a two-layer Couette flow over a deformable gel was studied [23]. They found two different interfacial modes. The first arose from the viscosity stratification at the liquid-liquid interface. The second was caused by a sudden jump in the shear modulus at the solid-liquid interface. It was shown that when the more viscous fluid had a smaller thickness, the solid layer completely stabilized the liquid-liquid interfacial mode. When the more viscous fluid had a larger thickness, the solid layer could either stabilize

*spush@iitm.ac.in

or destabilize the flow depending on the thickness of the solid layer. The role of wall deformability on the interfacial instabilities in gravity driven two-layer flows with a free surface was studied [24]. It was shown that three different interfacial modes evolve, i.e., gas-liquid, liquid-liquid, and solid-liquid modes. The solid deformability had a stabilizing effect on both gas-liquid and liquid-liquid modes when the more viscous liquid layer was near the deformable wall. When the less viscous liquid was adjacent to the deformable wall, the deformability always had a destabilizing effect on the liquid-liquid interfacial mode. Further increase in the solid deformability rendered all three interfacial modes unstable. Linear stability of core annular flows through deformable gel layers was studied [25]. It was shown that the gel layer had a stabilizing effect when the more viscous fluid was in the annular region.

From the above survey of the literature it is clear that very few studies have focused on two-phase pressure driven layered flows through soft-gel-coated walls. Understanding the underlying physics of this flow configuration is necessary to help in optimal design of microfluidic devices. In these systems the material is usually soft, like PDMS, and flows are typically pressure driven. Keeping this in mind our objective in this work is to carry out a linear stability analysis of two-phase layered flows through soft-gel-coated walls. Operating conditions which have a stabilizing or destabilizing effect on the liquid-liquid interfacial instability are identified. Insight into the dominant physical cause of different instabilities which occur is obtained using an energy budget analysis. In the present analysis we restrict ourselves to a linear viscoelastic model for the soft gel.

The outline of the paper is as follows. The governing equations, the steady state velocity fields of the fluids, and the displacement fields of the soft gels are presented in Secs. II and III. A description of linear stability analysis and energy budget analysis is given in Secs. IV and V. Section VI A discusses asymptotic results obtained by solving the governing equations in the long-wavelength limit. Appendix provides details of the asymptotic analysis used to obtain the growth rate in the long-wave limit. The numerical method used to obtain the dispersion curves and a comparison of the numerical method with the asymptotic analysis is discussed in Sec. VI B. Influence of gel layers on the stability characteristics of the long-wave mode is detailed in Sec. VI C. The Supplemental Material [26] details the results obtained using energy analysis for different operating conditions. The effect of parameters on different types of instabilities that arise are discussed in Secs. VI D, VI E, and VI F. Finally the key conclusions are summarized in Sec. VII.

II. GOVERNING EQUATIONS

The system being analyzed is a pressure driven layered flow of two immiscible liquids, "fluid 1" and "fluid 2," between two deformable soft-gel layers lining two parallel rigid surfaces. The schematic of the flow configuration is shown in Fig. 1. The two deformable soft-gel layers are assumed to be linear viscoelastic. The liquids are assumed to be incompressible and Newtonian. The nondimensional continuity and Navier-Stokes

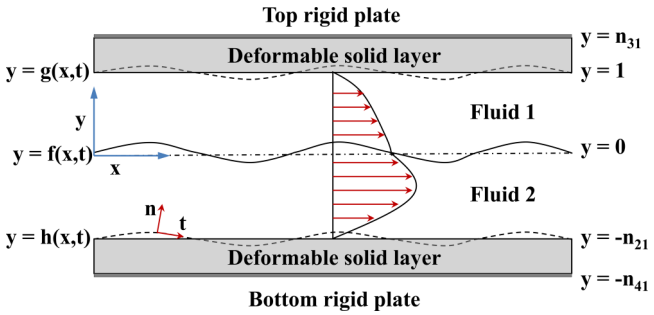

FIG. 1. Schematic of the flow configuration under study. At the base state, the liquid-liquid interface is at $y = 0$, top gel-liquid interface is at $y = 1$, and the bottom gel-liquid interface is at $y = -n_{21}$. The perturbed liquid-liquid interface is given by $y = f(x,t)$, the perturbed top gel-liquid interface is at $y = 1 + g(x,t)$, and the perturbed bottom gel-liquid interface is given by $y = -n_{21} + h(x,t)$. The parabolic velocity profile in the base state for the two fluids is also shown.

equations governing the flow are

$$\partial_x u_j + \partial_y v_j = 0, \tag{1}$$

$$\frac{\mathrm{Re}_1 \rho_{j1}}{\mu_{j1}}(\partial_t u_j + u_j \partial_x u_j + \partial_y u_j v_j) = \frac{-\mathrm{Re}_1}{\mu_{j1}}\partial_x p_j + \nabla^2 u_j, \tag{2}$$

$$\frac{\mathrm{Re}_1 \rho_{j1}}{\mu_{j1}}(\partial_t v_j + u_j \partial_x v_j + v_j \partial_y v_j) = \frac{-\mathrm{Re}_1}{\mu_{j1}}\partial_y p_j + \nabla^2 v_j, \tag{3}$$

where $j = 1, 2$ refers to the top and bottom fluids and ∂_t is $\partial/\partial t$ and ∂_x, ∂_y are similarly defined. The Laplacian $\nabla^2 = \partial_x^2 + \partial_y^2$. The variation of the dependent variables in the z direction is neglected as the system extends to infinity in that direction. We restrict ourselves to two-dimensional disturbances in the x-y plane in the present study.

In the governing equations (2) and (3) $\mathrm{Re}_1 = \rho_1 U_0 d_1/\mu_1$, $\mu_{j1} = \mu_j/\mu_1$, and $\rho_{j1} = \rho_j/\rho_1$, where d_1 is the thickness of fluid 1 and U_0 is the liquid-liquid interface velocity at the base state. The total stress tensor in the fluid layers is a combination of isotropic pressure and the deviatoric stresses. The liquid-liquid interface is located at $y = 0$ in the base state and the rigid walls are located at $y = n_{31}$, $y = -n_{41}$. The soft-gel layers extend from $1 < y < n_{31}$ and $-n_{41} < y < -n_{21}$.

The displacement fields in the deformable solid layers are considered to be small, justifying the linear viscoelastic solid model used here to capture the dynamics in the gel layers [14]. This deformation is characterized by the displacement fields X_j and Y_j, which represent the deviation of the material points from their unstrained reference state in the x and y directions, respectively. The velocity field in the deformable gel layer is given by $u_j = \partial_t X_j$, $v_j = \partial_t Y_j$. The nondimensional continuity and momentum equations for the top and bottom deformable solid layers are

$$\partial_x X_j + \partial_y Y_j = 0, \tag{4}$$

$$\frac{-\mathrm{Re}_1}{\mu_{j1}}\partial_x p_j + \frac{1}{\mathrm{Wi}_j}\nabla^2 X_j + \partial_t \nabla^2 X_j = 0, \tag{5}$$

$$\frac{-\mathrm{Re}_1}{\mu_{j1}}\partial_y p_j + \frac{1}{\mathrm{Wi}_j}\nabla^2 Y_j + \partial_t \nabla^2 Y_j = 0, \tag{6}$$

where $j = 3,\ 4$ refers to the top and bottom deformable soft-gel layers. The stress in the deformable layers comprises the isotropic pressure, elastic stresses, and viscous stresses. In Eqs. (5) and (6), the second and third terms represent the elastic stresses and the viscous stresses in the soft-gel layers. Here $\mu_{j1} = \mu_j/\mu_1$ is the ratio of gel viscosity to fluid 1 viscosity. Here, the nondimensional parameter Weissenberg number $\mathrm{Wi}_j = \mu_j U_0/G_j d_1$ is a measure of the deformable nature of the gel layers. The shear modulus G_j and viscosity μ_j are of the soft-gel layer under consideration. A higher Weissenberg number represents a higher deformability of the soft-gel layers. When the Weissenberg number approaches zero the deformable soft gels mimic the behavior of rigid solids.

The governing equations (1)–(6) are solved subject to the classical boundary conditions: At the liquid-liquid and gel-liquid interface, we use the continuity of velocities, tangential stresses, and normal stresses. The displacement field of the soft gel defines the shape of the perturbed interface. However, motion of the liquid-liquid interface $y = f(x,t)$ is captured by the kinematic boundary condition

$$D_t f = 0. \tag{7}$$

III. BASE STATE

The deformable soft-gel layers are considered to be at rest in the base state and the no-slip condition is employed at the gel-liquid interface. Also the gel layers are nonporous and fluid cannot penetrate the gel-liquid interfaces. The base velocity consists of parabolic profiles in each fluid. When nondimensionalized by the interfacial velocity U_0, this results in

$$U_1 = 1 + a_1 y + b_1 y^2, \tag{8}$$

$$U_2 = 1 + a_2 y + b_2 y^2, \tag{9}$$

where

$$a_1 = \frac{\mu_{21} - n_{21}^2}{n_{21}^2 + n_{21}}, \quad b_1 = -\frac{\mu_{21} + n_{21}}{n_{21}^2 + n_{21}}, \tag{10}$$

$$a_2 = \frac{a_1}{\mu_{21}}, \quad b_2 = \frac{b_1}{\mu_{21}}, \tag{11}$$

where $n_{21} = \frac{d_2}{d_1}$ is the thickness ratio of fluid 2 to fluid 1. The base state velocity expressions are identical to that of two-phase layered flow between rigid plates [27].

The base displacement fields in the top and bottom soft gels are given, respectively, by

$$X_3^{ss} = \frac{d_x p_0 d_1}{2G}\left\{y^2 + \left[\frac{n_{21}^2 - \mu_{21}}{n_{21} + \mu_{21}}\right]y - \frac{n_{31}[n_{21}(n_{21} + n_{31}) + \mu_{21}(n_{31} - 1)]}{n_{21} + \mu_{21}}\right\}, \tag{12}$$

$$X_4^{ss} = \frac{d_x p_0 d_1}{2G}\left\{y^2 + \left[\frac{n_{21}^2 - \mu_{21}}{n_{21} + \mu_{21}}\right]y - \frac{n_{41}[n_{21}(n_{41} - n_{21}) + \mu_{21}(n_{41} + 1)]}{n_{21} + \mu_{21}}\right\}, \tag{13}$$

where X_3^{SS} and X_4^{SS} represent the base state displacement fields and $d_x p_0$ is the pressure gradient in the flow direction in the gel. The displacements in the gel in the y direction are zero; i.e., $Y_3^{ss} = Y_4^{ss} = 0$. The expressions in Eqs. (12) and (13) are obtained by imposing no displacement of the soft gel in the flow direction at the rigid walls $y = n_{31}$ and $y = -n_{41}$ and continuity of tangential stress at the gel-liquid interfaces at $y = 1$ and $y = -n_{21}$.

IV. LINEAR STABILITY ANALYSIS

A temporal linear stability analysis is used to analyze the stability of the steady state. Small perturbations in normal mode form are imposed on all the variables (denoted by the tilde),

$$\begin{Bmatrix} u_i \\ v_i \\ p_i \end{Bmatrix} = \begin{Bmatrix} u_i^{ss} + \varepsilon\tilde{u}_i \\ v_i^{ss} + \varepsilon\tilde{v}_i \\ p_i^{ss} + \varepsilon\tilde{p}_i \end{Bmatrix}, \quad \text{where} \quad i = 1,2, \tag{14}$$

and

$$\begin{Bmatrix} X_j \\ Y_j \\ p_j \end{Bmatrix} = \begin{Bmatrix} X_j^{ss} + \varepsilon\tilde{X}_i \\ Y_j^{ss} + \varepsilon\tilde{Y}_i \\ p_j^{ss} + \varepsilon\tilde{p}_j \end{Bmatrix}, \quad \text{where} \quad j = 3,4. \tag{15}$$

The perturbed quantities are expanded as Fourier modes along the x direction with an exponential dependence on time. The perturbation for the axial component of velocity u_j is of the form

$$\tilde{u}_j = \bar{u}_j(y)\exp[ik(x - ct)]. \tag{16}$$

A similar form of perturbation is used for all the other variables. Here k is real and is the wave number and c is a complex wave speed. $\bar{u}_i$ is obtained as the eigenfunction of a linearized eigenvalue problem. The complex wave speed $c = c_R + ic_I$. Here c_R represents the phase velocity of the perturbation and c_I represents the growth or decay rate of the perturbations. The base state around which linear stability analysis is carried out is temporally unstable when $kc_I > 0$.

The linearized governing equations (1)–(3) for the fluids after substituting the form of perturbations in Eq. (16) (the bar is dropped for convenience) for $j = 1,\ 2$ are

$$iku_j + \frac{dv_j}{dy} = 0, \tag{17}$$

$$\frac{\mathrm{Re}_1\rho_{j1}}{\mu_{j1}}\left[-ikcu_j + U_j iku_j + \frac{dU_j}{dy}v_j\right] = \frac{-ik\mathrm{Re}_1}{\mu_{j1}}p_j + \left[\frac{d^2u_j}{dy^2} - k^2u_j\right], \tag{18}$$

$$\frac{\mathrm{Re}_1\rho_{j1}}{\mu_{j1}}[-ikcv_j + U_j ikv_j] = \frac{-ik\mathrm{Re}_1}{\mu_{j1}}\frac{dp_j}{dy} + \left[\frac{d^2v_j}{dy^2} - k^2v_j\right]. \tag{19}$$

In a similar way, the linearized equations for the top and bottom deformable soft gels for $j = 3,\ 4$ are

$$ikX_j + \frac{dY_j}{dy} = 0, \tag{20}$$

$$\frac{-\mathrm{Re}_1}{\mu_{j1}} ikp_j + \frac{1}{\mathrm{Wi}_j}\left[\frac{d^2X_j}{dy^2} - k^2X_j\right] + \left[ick^3X_j - ikc\frac{d^2X_j}{dy^2}\right] = 0, \quad (21)$$

$$\frac{-\mathrm{Re}_1}{\mu_{j1}} \frac{dp_j}{dy} + \frac{1}{\mathrm{Wi}_j}\left[\frac{d^2Y_j}{dy^2} - k^2Y_j\right] + \left[ick^3Y_j - ikc\frac{d^2Y_j}{dy^2}\right] = 0. \quad (22)$$

The boundary conditions at the perturbed liquid-liquid interface,

$$y = f(x,t) = \varepsilon\delta \exp[ik(x - ct)], \quad (23)$$

are obtained using domain perturbation [28]. Here δ is the amplitude of the perturbed liquid-liquid interface. The continuity of velocity yields

$$u_1 + \frac{dU_1}{dy}\delta = u_2 + \frac{dU_2}{dy}\delta, \quad (24)$$

$$v_1 = v_2. \quad (25)$$

The continuity of shear stress gives

$$\frac{du_1}{dy} + ikv_1 = \mu_{21}\left(\frac{du_2}{dy} + ikv_2\right). \quad (26)$$

The normal stress boundary condition yields

$$\mathrm{Re}_1(p_2 - p_1) + 2\frac{dv_1}{dy} - 2\mu_{21}\frac{dv_2}{dy} = \mathrm{Re}_1 S_{21}k^2\delta. \quad (27)$$

The kinematic boundary condition yields

$$\delta(ikc - U_1ik) + v_1 = 0. \quad (28)$$

The nondimensional parameter S_{21} in Eq. (27) is defined as $S_{21} = \sigma_{21}/\rho_1 d_1 U_0^2$. It represents the ratio of forces due to surface tension (σ) between the liquids due to the inertial forces. The above equations (24)–(28) are evaluated at $y = 0$, the unperturbed interface.

The shapes of the perturbed top and bottom gel-liquid interfaces are given by

$$y = 1 + \varepsilon g(x,t) = 1 + \varepsilon Y_3 \exp[ik(x - ct)],$$
$$y = -n_{21} + \varepsilon h(x,t) = -n_{21} + \varepsilon Y_4 \exp[ik(x - ct)]. \quad (29)$$

The boundary conditions at the perturbed gel-liquid interface at $y = 1$ are obtained after linearization and applying domain perturbation. These yield, at $y = 1$,

$$u_1 + \frac{dU_1}{dy}Y_3 = -ikcX_3, \quad (30)$$

$$v_1 = -ikcY_3, \quad (31)$$

$$\frac{1}{\mu_{31}}\left(\frac{du_1}{dy} + ikv_1\right) = \frac{1}{\mathrm{Wi}_3}\left[\frac{dX_3}{dy} + ikY_3\right] + \left[-ikc\frac{dX_3}{dy} + k^2cY_3\right], \quad (32)$$

$$\mathrm{Re}_1(p_1 - p_3) + \frac{2\mu_{31}}{\mathrm{Wi}_3}\frac{dY_3}{dy} + 2\left(\mu_{31}ikc\frac{dY_3}{dy}\right) - 2\frac{\partial v_1}{\partial y} = \mathrm{Re}_1 S_{31}k^2Y_3. \quad (33)$$

Similar boundary conditions are applicable at the gel-liquid interface at $y = -n_{21}$. In Eq. (33) the dimensionless parameter S_{31} is defined as $S_{31} = \sigma_{31}/\rho_1 d_1 U_0^2$. At $y = n_{31}$ and $y = -n_{41}$ we have rigid walls on which the gel layers are coated. This yields

$$X_3 = 0; \quad Y_3 = 0 \ \text{ at } \ y = n_{31},$$
$$X_4 = 0; \quad Y_4 = 0 \ \text{ at } \ y = -n_{41}. \quad (34)$$

The stability of layered flow between two walls with a soft-gel lining is completely defined by the governing equations (17)–(22) and boundary conditions given by Eqs. (23)–(34). The growth rate of the disturbance kc_I is a function of n_{21}, n_{31}, n_{41}, ρ_{21}, μ_{21}, μ_{31}, μ_{41}, S_{21}, S_{31}, S_{41}, Wi_3, Wi_4, Re_1, and k. The above equations give rise to a generalized eigenvalue problem for c.

$$\boldsymbol{A}x = c\boldsymbol{B}x. \quad (35)$$

The linearized equations are solved numerically using the Chebyshev collocation technique for a range of k. kc_I, which corresponds to the growth rate of the disturbance, is analyzed to determine the stability of the flow.

V. ENERGY BUDGET

To understand the physical origin of the different modes of instability in the problem, we carry out an energy budget analysis. A detailed description of the theory behind energy analysis is given in [4,29]. Here we take the inner product of the vectorial form of the Navier-Stokes equation with the velocity vector and integrate throughout the domain in each of the fluid and solid layers. The entire equation is averaged over the axial wavelength $\lambda = 2\pi/k$ and time period $T = 2\pi/kc_R$. The stress terms in the energy analysis are analyzed using the Gauss divergence theorem. This gives rise to the following equation:

$$\sum_{j=1}^{2} E_{\mathrm{KE},j} = \sum_{j=1}^{2} E_{\mathrm{REY},j} + \sum_{j=1}^{3} E_{\mathrm{NOR},j} + \sum_{j=1}^{3} E_{\mathrm{TAN},j} + \sum_{j=1}^{4} E_{\mathrm{DIS},j}, \quad (36)$$

$$E_{\mathrm{KE},j} = \frac{\rho_{j1}}{\lambda}\int_0^T\int_0^\lambda\int_{\alpha_j}^{\beta_j}\left[\frac{d}{dt}\left(\frac{u_j^2 + v_j^2}{2}\right)\right]dydxdt, \quad (37)$$

$$E_{\mathrm{REY},j} = \frac{-\rho_{j1}}{\lambda}\int_0^T\int_0^\lambda\int_{\alpha_j}^{\beta_j}\left[u_jv_j\frac{dU_j}{dy}\right]dydxdt, \quad (38)$$

$$E_{\mathrm{DIS},j} = \frac{-\mu_{j1}}{\mathrm{Re}_1\lambda}\int_0^T\int_0^\lambda\int_{\alpha_j}^{\beta_j}\left[2\left(\frac{\partial u_j}{\partial x}\right)^2 + 2\left(\frac{\partial v_j}{\partial y}\right)^2 + \left(\frac{\partial u_j}{\partial y} + \frac{\partial v_j}{\partial x}\right)^2\right]dydxdt. \quad (39)$$

The above three expressions are valid for $j = 1, 2$. For $j = 3, 4$ we have

$$E_{\mathrm{DIS},j} = \frac{-\mu_{j1}}{\mathrm{Re}_1\lambda}\int_0^T\int_0^\lambda\int_{\alpha_j}^{\beta_j}\left[2\left(\frac{1}{\mathrm{Wi}_j}+\frac{\partial}{\partial t}\right)\left(\frac{\partial X_j}{\partial x}\frac{\partial^2 X_j}{\partial x\partial t}+\frac{\partial Y_j}{\partial y}\frac{\partial^2 Y_j}{\partial y\partial t}\right)\right] + \left\{\left(\frac{1}{\mathrm{Wi}_j}+\frac{\partial}{\partial t}\right)\left(\frac{\partial X_j}{\partial y}+\frac{\partial Y_j}{\partial x}\right)\left[\frac{\partial}{\partial t}\left(\frac{\partial X_j}{\partial y}+\frac{\partial Y_j}{\partial x}\right)\right]\right\} dy dx dt. \tag{40}$$

The terms at the different interfaces are

$$E_{\mathrm{NOR},1} = \frac{1}{\lambda}\int_0^T\int_0^\lambda\left[p_1 v_1 - p_2 v_2 - \frac{2v_1}{\mathrm{Re}_1}\frac{dv_1}{dy} + \frac{2\mu_{21}v_2}{\mathrm{Re}_1}\frac{dv_2}{dy}\right]_{y=0} dx dt, \tag{41}$$

$$E_{\mathrm{NOR},2} = \frac{1}{\lambda}\int_0^T\int_0^\lambda\left[p_3\frac{\partial Y_3}{\partial t} - p_1 v_1 + \frac{2v_1}{\mathrm{Re}_1}\frac{dv_1}{dy} - \frac{2\mu_{31}}{\mathrm{Re}_1}\frac{\partial Y_3}{\partial t}\left(\frac{1}{\mathrm{Wi}_3}\frac{\partial Y_3}{\partial y}+\frac{\partial}{\partial t}\frac{\partial Y_3}{\partial y}\right)\right]_{y=1} dx dt, \tag{42}$$

$$E_{\mathrm{NOR},3} = \frac{1}{\lambda}\int_0^T\int_0^\lambda\left[-p_4\frac{\partial Y_4}{\partial t} + p_2 v_2 - \frac{2\mu_{21}v_2}{\mathrm{Re}_1}\frac{dv_2}{dy} + \frac{2\mu_{41}}{\mathrm{Re}_1}\frac{\partial Y_4}{\partial t}\left(\frac{1}{\mathrm{Wi}_4}\frac{\partial Y_4}{\partial y}+\frac{\partial}{\partial t}\frac{\partial Y_4}{\partial y}\right)\right]_{y=-n_{21}} dx dt, \tag{43}$$

$$E_{\mathrm{TAN},1} = \frac{1}{\mathrm{Re}_1\lambda}\int_0^T\int_0^\lambda\left[(u_2-u_1)\left(\frac{\partial u_1}{\partial y}+\frac{\partial v_1}{\partial x}\right)\right]_{y=0} dx dt, \tag{44}$$

$$E_{\mathrm{TAN},2} = \frac{1}{\mathrm{Re}_1\lambda}\int_0^T\int_0^\lambda\left[u_1\left(\frac{\partial u_1}{\partial y}+\frac{\partial v_1}{\partial x}\right) - \frac{\mu_{31}}{\mathrm{Wi}_3}\left(\frac{\partial X_3}{\partial y}+\frac{\partial Y_3}{\partial x}\right) - \frac{\partial}{\partial t}\left(\frac{\partial X_3}{\partial y}+\frac{\partial Y_3}{\partial x}\right)\right]_{y=1} dx dt, \tag{45}$$

$$E_{\mathrm{TAN},3} = \frac{1}{\mathrm{Re}_1\lambda}\int_0^T\int_0^\lambda\left[-\mu_{21}u_2\left(\frac{\partial u_2}{\partial y}+\frac{\partial v_2}{\partial x}\right) + \frac{\mu_{41}}{\mathrm{Wi}_4}\left(\frac{\partial X_4}{\partial y}+\frac{\partial Y_4}{\partial x}\right) - \frac{\partial}{\partial t}\left(\frac{\partial X_4}{\partial y}+\frac{\partial Y_4}{\partial x}\right)\right]_{y=-n_{21}} dx dt. \tag{46}$$

In Eqs. (37)–(46) $\alpha_1 = 0, \beta_1 = 1, \alpha_2 = 0, \beta_2 = -n_{21}, \alpha_3 = 1, \beta_3 = n_{31}, \alpha_4 = -n_{21}, \beta_4 = -n_{41}$. The term on the left-hand side of Eq. (36) represents the kinetic energy of the disturbance in the system. We do not consider the inertial terms in the linear viscoelastic model for the deformable gels. Hence the gels do not contribute to the kinetic energy in the energy budget. A positive value of this term indicates the flow is unstable. The four terms on the right-hand side are contributions from the Reynolds stresses, normal stress, tangential stress, and viscous dissipation. The term $\sum_{j=1}^{2} E_{E_{\mathrm{REY},j}}$ represents the total energy transferred from the base state to the perturbed state due to Reynolds stresses in the fluids. This term is significant at higher Re_1. Since, we do not incorporate inertial effects of the deformable gels in the linear viscoelastic model, Reynolds stresses of the gel layers do not contribute to the total energy. The term $\sum_{j=1}^{2} E_{\mathrm{DIS,j}}$ represents the viscous dissipation in the fluids and is always negative. The term $\sum_{j=3}^{4} E_{\mathrm{DIS,j}}$ represents the viscous dissipation in the deformable solid layers due to its liquidlike nature and is always negative. The term $E_{\mathrm{NOR},1}$ represents the capillary forces at the liquid-liquid interface, whereas the terms $E_{\mathrm{NOR},2}$, $E_{\mathrm{NOR},3}$ represent the capillary forces at the top and bottom gel-liquid interfaces. The term $E_{\mathrm{TAN},1}$ is associated with the viscosity difference between the fluids, as a result of which energy is transferred from the base state to the perturbed state and can cause an instability at low Re_1 [5]. The terms $E_{\mathrm{TAN},2}$ and $E_{\mathrm{TAN},3}$ not only arise from a viscosity difference but also from a discontinuity in the shear modulus across the gel-liquid interfaces. This discontinuity in the shear modulus gives rise to additional instabilities in the flow.

The energy budget helps us to understand the dominant physical mechanism which causes the instability. The eigenfunctions obtained by solving the linearized equations are substituted into the expressions in (36)–(46). The term with the largest magnitude dominates the energy signature. If the contribution of an energy term is negative (positive) this implies it has a stabilizing (destabilizing) effect on the system. The largest positive term indicates the primary or dominant cause of the instability.

VI. RESULTS

In this section, the stability of the base flow configuration to arbitrary disturbances is analyzed. The effect of varying parameters on dispersion curves is studied systematically. An energy budget analysis is used to obtain insights into the physical mechanism causing the different instabilities for the most unstable growth rate.

We begin by summarizing the results of layered flows between rigid-walled channels [27]. From the long-wave analysis of [27], we conclude that the flow is unstable when $(\mu_{21} - n_{21}^2)(\mu_{21} - 1) > 0$. This long-wave instability is also referred to as an interfacial mode and results in the destabilization of the liquid-liquid interface. This is labeled as the "LL long-wave mode." The parameter space μ_{21}-n_{21} is divided into four different regions by curves across which the stability to this mode changes as shown in Fig. 2. In regions 1 and 3, the steady state is unstable to the LL long-wave mode while in regions 2 and 4 it is stable.

The flow can also be unstable to short-wave modes. This is referred to as shear mode of the Tollmien-Schlichting type, which occurs for a relatively large Reynolds number. We label this as the "LL short-wave mode."

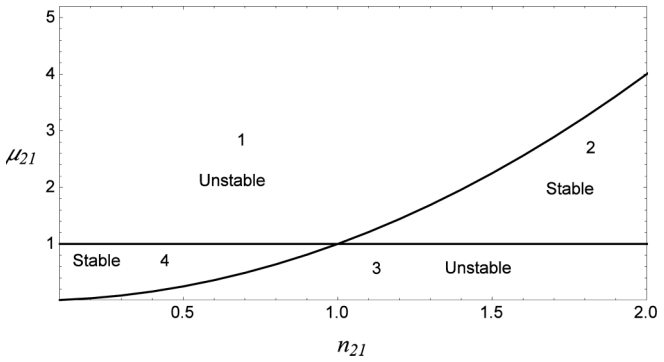

FIG. 2. Stability features in different regions in μ_{21}-n_{21} parameter space for two-phase layered flow between rigid flat plates.

Apart from these, the deformable gels at the top and bottom walls can give rise to an additional short-wave instability at the gel-liquid interface as reported in [13,23]. We call this the "GL short-wave mode."

A. Long-wave analysis for gel-coated walls

We use a long-wave analysis as discussed in [27] and obtain an asymptotic solution to the eigenvalue problem using a series expansion in k, in the limit of long-wavelength ($k \to 0$). This is used to obtain physical insight on the effect of deformability of soft-gel layers on the stability of the base state to the LL long-wave mode. In the asymptotic analysis the primary assumption is that the wavelength of the disturbance is much larger than the thickness of various layers of the fluids and gels present; i.e., $k \ll \frac{1}{n_{31}+n_{41}}$. The complex wave speed is expanded in an asymptotic series in k as

$$c = c^{(0)} + kc^{(1)} + \cdots . \tag{47}$$

To focus on the effect of gel on the stability of the liquid-liquid interface, we assume Re_1 and Wi_3, Wi_4 to be $O(1)$. We set $v_j \sim O(1)$. Then the continuity Eq. (17) implies $u_j \sim v_j/k$ and the x momentum Eq. (18) implies $p_j \sim v_j/k^2$. Using this, the velocities and the pressure in the liquids are expanded in an asymptotic series in k as

$$v_j = v_j^{(0)} + kv_j^{(1)} + \cdots , \tag{48}$$

$$u_j = \frac{u_j^{(0)}}{k} + u_j^{(1)} + \cdots , \tag{49}$$

$$p_j = \frac{p_j^{(0)}}{k^2} + \frac{p_j^{(1)}}{k} + \cdots . \tag{50}$$

For our system the first order term $c^{(1)}$ in Eq. (47) helps capture the effect of k on the stability of the system for low wave numbers. The displacement fields and pressure in the soft gels are expanded in an asymptotic series in k as

$$Y_j = Y_j^{(0)} + kY_j^{(1)} + \cdots , \tag{51}$$

$$X_j = \frac{X_j^{(0)}}{k} + X_j^{(1)} + \cdots , \tag{52}$$

$$p_j = \frac{p_j^{(0)}}{k^2} + \frac{p_j^{(1)}}{k} + \cdots . \tag{53}$$

The leading order displacement fields and pressure fields for the soft-gel layers suffice to carry out the long-wave asymptotic analysis. To first order we obtain, for the growth rate,

$$kc = kc^{(0)} + k^2c^{(1)},$$
$$kc = k\left\{1 + \left[\frac{2(\mu_{21} - n_{21}^2)(\mu_{21} - 1)(n_{21}^3 + n_{21}^2)}{(n_{21}^2 + n_{21})(n_{21}^4 + 4n_{21}^3\mu_{21} + 6n_{21}^2\mu_{21} + 4n_{21}\mu_{21} + \mu_{21}^2)}\right]\right\} + k^2c^{(1)}. \tag{54}$$

The details of the derivation of this expression are given in Appendix. The term in the square braces in Eq. (54) is the wave speed of the disturbance of wave number k. The growth rate of the disturbance to this order is given by the imaginary part of kc. This is a function of all parameters which describe the system. To gain insight into the influence of the elasticity of the gels, we fix ρ_{21}, n_{21}, μ_{21}, μ_{31}, μ_{41}, n_{31}, and n_{41}. The dependency of growth rate explicitly on Re_1, Wi_3, and Wi_4 is of the form

$$\mathrm{Im}(c^{(1)}) = a_1\mathrm{Re}_1 + b_3\mathrm{Wi}_3 + b_4\mathrm{Wi}_4. \tag{55}$$

Here a_1, b_3, and b_4 are coefficients which depend on ρ_{21}, n_{21}, μ_{21}, μ_{31}, μ_{41}, n_{31}, and n_{41}. In the long-wavelength limit, the parameters S_{21}, S_{31}, and S_{41} do not influence a_1, b_3, and b_4.

B. Comparison of long-wave analysis and numerical results

We follow [30,31] and use a Chebyshev collocation technique to numerically solve the eigenvalue problem for arbitrary wave numbers. The variables u_j, v_j, X_j, Y_j are expressed as a sum of Chebyshev polynomials up to degree N and the pressures in the fluids and the solids are expressed as a sum of Chebyshev polynomials up to degree N–2 [32]. Equations for the coefficients in the expansions are obtained by collocating the governing equations in the internal Gauss-Lobatto points and the boundary conditions are evaluated at the end nodes of the Gauss-Lobatto grid. This results in a generalized matrix eigenvalue problem of the form $\boldsymbol{A}x = c\boldsymbol{B}x$. The eigenvalues are obtained using the QZ algorithm. Numerical calculations were carried out for $N = 20$, 30, and 40. The eigenvalues computed were found to be invariant for N beyond 30. All the results presented here are for $N = 30$. In the limit of $\mathrm{Wi}_3 \to 0$ and $\mathrm{Wi}_4 \to 0$, the present flow configuration reduces to layered flow between rigid flat plates described in [27]. The results obtained from the numerical simulations in this limit are validated by comparing our results with those mentioned in [27]. A comparison of the dispersion curves

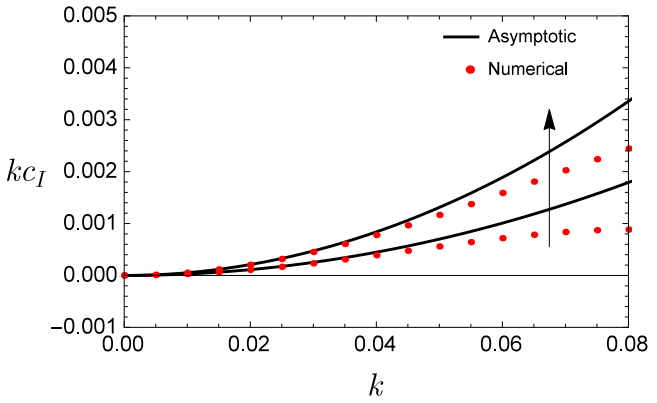

FIG. 3. Comparison of dispersion curves obtained from long-wave asymptotic analysis and numerical simulations for $\mathrm{Re}_1 = 6,8$. The arrow points in the direction of increasing Reynolds number. Other parameters: $n_{21} = 1, n_{31} = 1.5, n_{41} = 1.5$, $\mu_{21} = 0.1$, $\mu_{31} = 1$, $\mu_{41} = 1$, $\rho_{21} = 1.16$, $S_{31} = S_{41} = 0.0001$, $S_{21} = \frac{829}{\mathrm{Re}_1^2}$, $\mathrm{Wi}_3 = \mathrm{Wi}_4 = 0.5$.

obtained numerically with those obtained from the long-wave asymptotic analysis using Eq. (54) is shown in Fig. 3. It can be seen that the first order correction in the asymptotic analysis captures the growth rate accurately for $k < 0.055$ for $\mathrm{Re}_1 = 6$ and $k < 0.045$ for $\mathrm{Re}_1 = 8$.

C. Influence of gel on the stability of the behavior of LL long-wave mode

In Fig. 4(a) the parameter space μ_{21}-n_{21} is divided into different regions by curves across which the coefficients b_3 and b_4 multiplying Wi_3 and Wi_4 in Eq. (55) change sign for a fixed ρ_{21}, n_{21}, μ_{21}, μ_{31}, μ_{41}, n_{31}, and n_{41}. A region where a coefficient is positive (negative) indicates that the corresponding gel layer may have a destabilizing (stabilizing) effect on the LL long-wave mode.

In regions (i), (iii), and (vi) both the coefficients are negative indicating a stabilizing effect of the gels on the LL long-wave mode. In region (ii) b_3 is positive and b_4 is negative, indicating that the top (bottom) gel has a destabilizing (stabilizing) effect.

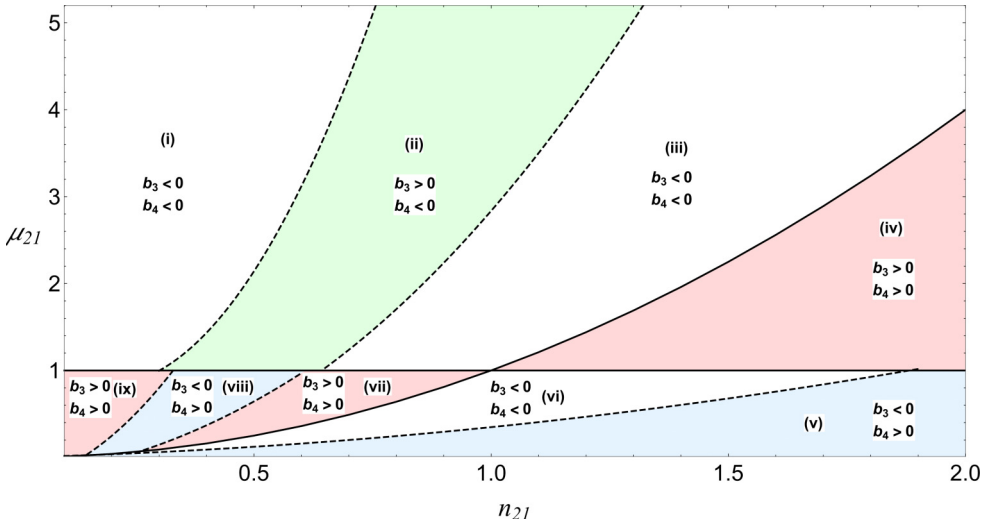

(a)

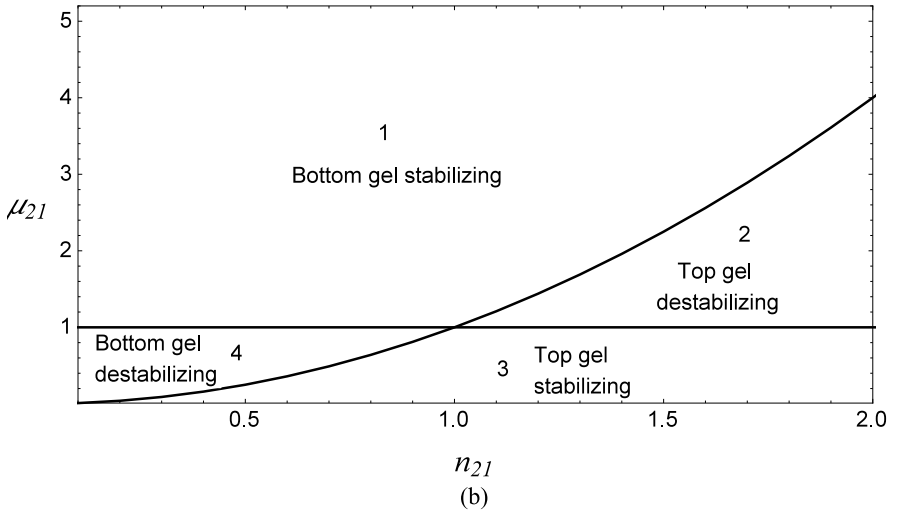

(b)

FIG. 4. (a) Division of parameter space into different regions where each region has a specific sign of coefficients b_3 and b_4 in Eq. (55). (b) Dominant influence on stability in different regions. Parameters: $n_{31} = 2$, $n_{41} = 2$, $\mu_{31} = 1$, $\mu_{41} = 1$, $\rho_{21} = 1.16$.

In regions (iv), (vii), and (ix) both the coefficients are positive, indicating that both have a destabilizing effect on this mode. In regions (v) and (viii) b_3 is negative and b_4 is positive, indicating that the top (bottom) gel has a stabilizing (destabilizing) effect on the LL long-wave mode. In regions (i), (ii), and (iii) our numerical calculations show that the bottom gel has a strong stabilizing effect since $|b_4| > |b_3|$. Similarly in region (iv) the top gel has a predominantly destabilizing effect since $|b_3| > |b_4|$. In regions (v) and (vi) the top gel has a strong stabilizing behavior as $|b_3| > |b_4|$. In regions (vii), (viii), and (ix) the bottom gel has a predominantly destabilizing effect as $|b_4| > |b_3|$. On the basis of the observations based on numerical evaluations the parameter space in Fig. 4(b) is divided into different regions showing the predominant effect of the gels on stability. In region 1 and region 3 the LL long-wave mode is unstable for two-phase layered flows between flat plates. Here having a gel close to the more viscous fluid has a stabilizing effect on the LL long-wave mode. In region 2 and region 4 the LL long-wave mode is stable for two-phase flow between rigid flat plates. Here the gel closer to the less viscous and narrower fluid has a destabilizing effect on the LL long-wave mode. Typical values of the coefficients b_3, b_4 for the growth rate obtained from long-wave analysis in each region in μ_{21}-n_{21} parameter space are discussed in the Supplemental Material [26]. Destabilization (stabilization) of the flow in regions 2 and 4 (regions 1 and 3) by the introduction of a soft-gel layer is analogous to the destabilization (stabilization) caused by the soft-gel layer in core annular flow when the less (more) viscous fluid occupies the annular region [25]. To summarize, introducing an appropriate soft-gel layer destabilizes the flow in regions 2 and 4 where the flow between rigid walls is stable. In regions 1 and 3 where the flow between rigid walls is unstable introducing an appropriate gel can have a stabilizing influence.

The influence of the gels on the LL long-wave mode in different regions can be physically explained using an energy budget analysis [4]. For this we choose the wave number corresponding to which the growth rate is a maximum. These are used to calculate the contribution of different energy terms to the disturbance. All the terms in the energy budget are normalized with the absolute value of total viscous dissipation. In region 1 and region 3: $E_{\mathrm{TAN},1}$ is the dominating term in the energy analysis indicating that the tangential stresses at the liquid-liquid interface leads to the evolution of the LL long-wave mode. With an increase in the corresponding Weissenberg number (Wi_3 and Wi_4), the magnitude of the $E_{\mathrm{TAN},1}$ term in the energy budget decreases relative to the viscous dissipation in the fluids and the gel layers. This stabilizes the LL long-wave mode. In region 2 and region 4 introduction of gels has a destabilizing influence. Here $E_{\mathrm{TAN},2}$ and $E_{\mathrm{TAN},3}$ are significant but are lower in magnitude compared to $E_{\mathrm{TAN},1}$. The latter is primarily responsible for the instability. The energy budget analysis is detailed in the Supplemental Material [26].

D. Numerical analysis of the effect of deformable gels on the LL long-wave mode

In this section we use the insight from the long-wave analysis and numerically analyze the influence of introducing a gel layer coating on the walls. The influence of different parameters on stability depicted in Fig. 4(b) is based on the long-wave analysis. The numerical results we now discuss correspond to region 3 in Fig. 4(b). Here we expect that an increase in the deformability of the top gel should stabilize the LL long-wave mode. From our asymptotic analysis we predict that this mode will be stabilized for small wave numbers. In Fig. 5 the numerical results show that the stabilizing influence prevails for all wave numbers. Here a large Wi_j represents higher deformability of the jth soft-gel layers. As we increase Wi_3 from 0.05 to 0.5 the maximum growth rate decreases. For $\mathrm{Wi}_3 = 1$, this mode is completely stabilized for all wave numbers; i.e., the growth rates for all the wave numbers are negative indicating that disturbances do not grow in time. For different Wi_3 values the results of energy analysis are provided in the Supplemental Material [26]. The dominant contribution to the kinetic energy at the wave number for which the growth rate is a maximum is from $E_{\mathrm{TAN},1}$, the tangential stress term at the liquid-liquid interface. This term induces instability at the liquid-liquid interface. The contribution of the tangential stresses $E_{\mathrm{TAN},2}$, $E_{\mathrm{TAN},3}$ at the top and bottom gel-liquid interface are relatively small. As Wi_3 increases, $E_{\mathrm{TAN},1}$ decreases relative to viscous dissipation. Therefore the deformable nature of the gels stabilizes the base state. The stabilization of this mode by introducing a bottom gel in region 1 in Fig. 4(b) can also be explained using similar arguments.

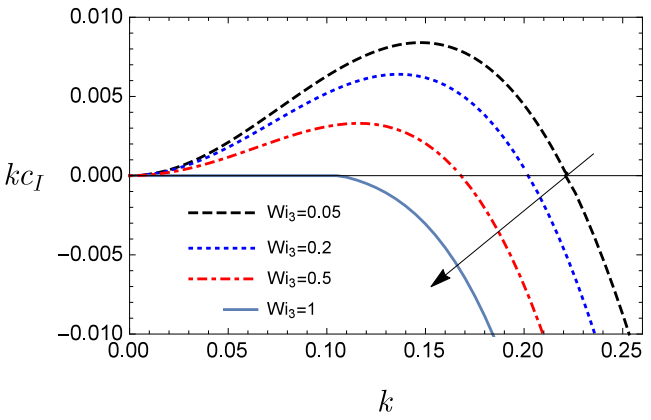

FIG. 5. Dispersion curves for the LL long-wave mode for $\mathrm{Wi}_3 = \mathrm{Wi}_4$ varying from 0.05 to 1 and $\mu_{21} = 0.1$. The arrow points in the direction of decreasing Weissenberg number. For $\mathrm{Wi}_3 = \mathrm{Wi}_4 = 1$ complete stabilization of the LL long-wave mode is observed. Other parameters: $n_{21} = 1$, $n_{31} = 1.5$, $n_{41} = 1.5$, $\mu_{31} = 1$, $\mu_{41} = 1$, $\rho_{21} = 1.16$, $\mathrm{Re}_1 = 8$, $S_{31} = S_{41} = 0.0001$, $S_{21} = \frac{829}{\mathrm{Re}_1^2}$.

We examine the axial velocity profiles in Fig. 6 and the stream function contours in Fig. 7. These are obtained from the eigenfunctions of the most unstable perturbation for $\mathrm{Wi}_3 = 0.05$ [33]. The velocity perturbations are discontinuous at the liquid-liquid interface because of the difference in the base state velocity gradient [see Eq. (24)]. The maximum of the axial velocity perturbation occurs at the interface as shown in Fig. 6. Figure 7 shows the two-dimensional (2D) contours of the stream function perturbation over one wavelength (for $0 \leqslant x \leqslant 2l_{\mathrm{wave}}$ where $l_{\mathrm{wave}} = 2\pi/k$). The gradient of the stream lines along the y direction increases as we approach the liquid-liquid interface. This is consistent with the axial

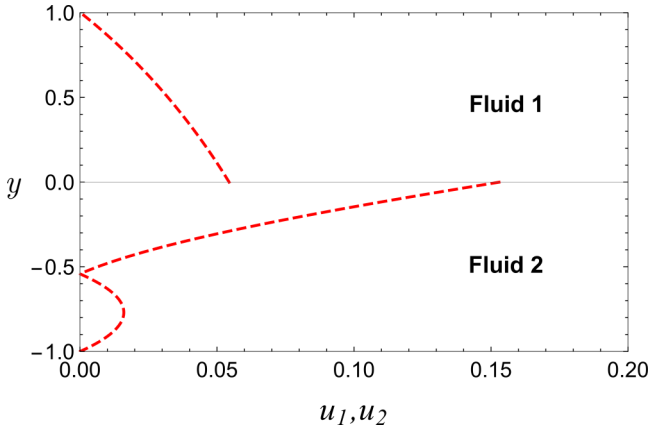

FIG. 6. The perturbed axial velocity for the LL long-wave mode of instability for $n_{21} = 1$, $n_{31} = 1.5$,$n_{41} = 1.5$, $\mu_{31} = 1$, $\mu_{41} = 1$, $\rho_{21} = 1.16$, $\mathrm{Re}_1 = 8$, $S_{31} = S_{41} = 0.0001$, $S_{21} = \frac{829}{\mathrm{Re}_1^2}$, $\mu_{21} = 0.1$, $\mathrm{Wi}_3 = \mathrm{Wi}_4 = 0.05$. The profiles are obtained for $x = 2\pi/k$.

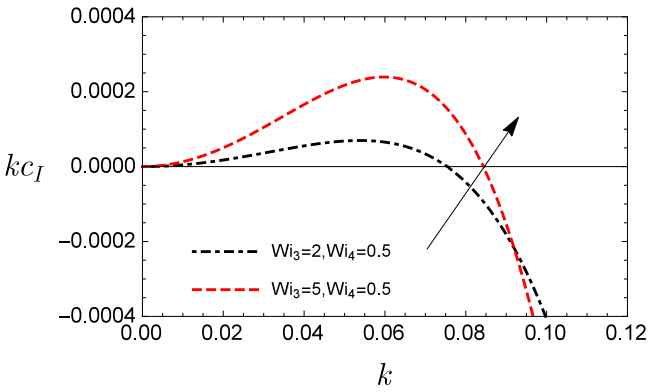

FIG. 8. Destabilization of LL long-wave mode. Parameters: $n_{21} = 1.76$, $n_{31} = 2$, $n_{41} = 2$, $\mu_{21} = 2$, $\mu_{31} = 1$, $\mu_{41} = 1$, $\rho_{21} = 1.16$, $\mathrm{Re}_1 = 8$, $S_{31} = S_{41} = 0.0001$, $S_{21} = \frac{829}{\mathrm{Re}_1^2}$. Arrow points in the direction of increasing Wi_3.

velocity perturbation being a maximum at the liquid-liquid interface. This indicates that the perturbation grows from the liquid-liquid interface in this mode.

An unexpected result is the destabilization of the LL long-wave mode in region 2 of Fig. 4(b) by introducing a gel. In Fig. 8 the maximum growth rate of the disturbances increases as we increase Wi_3, keeping Wi_4 fixed. This confirms the destabilizing influence of the top gel in region 2. The results from the energy analysis for this case are provided in the Supplemental Material [26]. The destabilization in this region is due to the additional stresses created at the top gel-liquid interface, i.e., $E_{\mathrm{TAN},2}$. A similar analysis for parameters in region 4 shows that the stresses at the bottom gel-liquid interface can cause a dominant destabilization effect. Regions 2 and 4 which were stable to this mode for flow between rigid walls have become unstable by introduction of a gel.

E. Destabilization of LL short-wave mode

In this section, we analyze the effect of deformable walls on the liquid-liquid short-wave mode [27]. This mode is unstable for large wave numbers and hence long-wave asymptotic analysis cannot be used to get insights into this instability. In Figs. 9(a) and 9(b) we see that this mode is destabilized by an increase in the deformable nature of the soft gel for different viscosity ratios and Reynolds numbers. When the Weissenberg numbers of the top and bottom deformable gels are equal and increased from 0.05 to 0.25 the maximum growth rate increases. The energy budget analysis for this instability is shown in Table I. Here the $\sum_{j=1}^{2} E_{\mathrm{REY},j}$ term; i.e., Reynolds

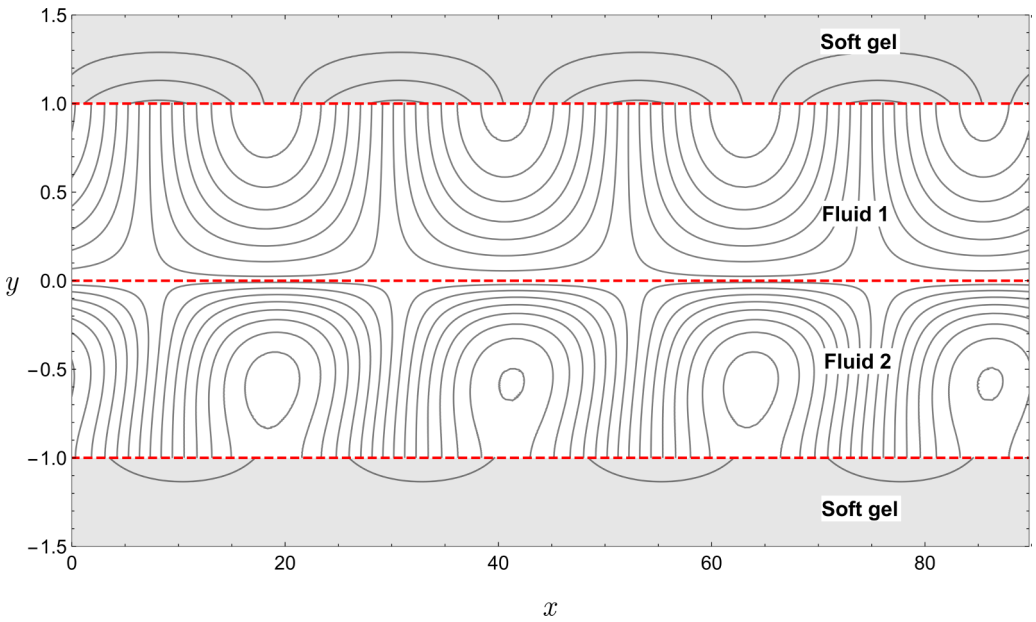

FIG. 7. Contours of perturbed stream function for the LL long-wave instability for $0 \leqslant x \leqslant 2l_{\mathrm{wave}}$ and $-1 \leqslant y \leqslant 1$ where $l_{\mathrm{wave}} = 2\pi/k$. Other parameters: $n_{21} = 1$, $n_{31} = 1.5$,$n_{41} = 1.5$, $\mu_{31} = 1$, $\mu_{41} = 1$, $\rho_{21} = 1.16$, $\mathrm{Re}_1 = 8$, $S_{31} = S_{41} = 0.0001$, $S_{21} = \frac{829}{\mathrm{Re}_1^2}$, $\mu_{21} = 0.1$, $\mathrm{Wi}_3 = \mathrm{Wi}_4 = 0.05$.

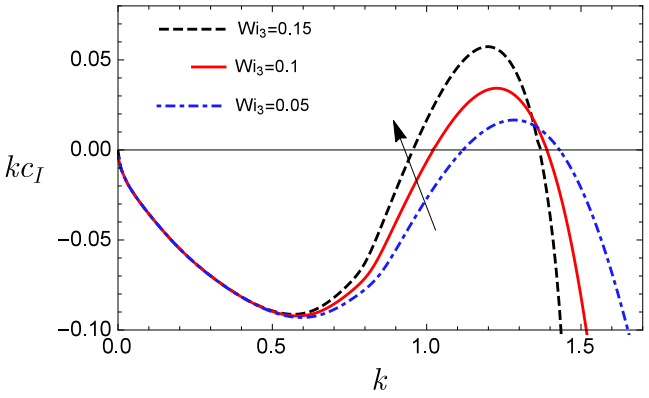

FIG. 9. Dispersion curves for the LL short-wave mode for $\mathrm{Wi}_3 = \mathrm{Wi}_4$ varying from 0.05 to 0.25 and (a) $\mu_{21} = 0.05$, $\mathrm{Re}_1 = 230$; (b)$\mu_{21} = 0.1$, $\mathrm{Re}_1 = 700$. The arrow points in the direction of increasing Wi_3. Other parameters: $n_{21} = 1, n_{31} = 1.5, n_{41} = 1.5$, $\mu_{31} = 10, \mu_{41} = 10, \rho_{21} = 1.16, S_{21} = \frac{829}{\mathrm{Re}_1^2}, S_{31} = S_{41} = 0.0001$.

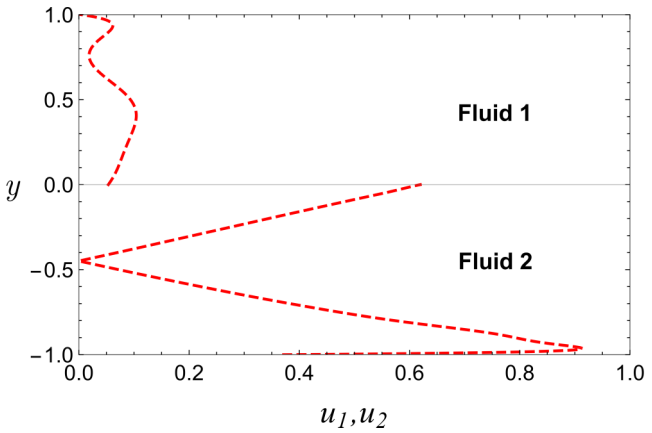

FIG. 10. The perturbed axial velocity for the LL short-wave mode instability for $n_{21} = 1$, $n_{31} = 1.5$, $n_{41} = 1.5$, $\mu_{31} = 10$, $\mu_{41} = 10$, $\rho_{21} = 1.16$, $\mathrm{Re}_1 = 700$, $S_{31} = S_{41} = 0.0001$, $S_{21} = \frac{829}{\mathrm{Re}_1^2}$, $\mu_{21} = 0.1$, $\mathrm{Wi}_3 = \mathrm{Wi}_4 = 0.2$. The profiles are obtained for $x = 2\pi/k$.

stresses in the fluids, makes a dominant contribution to the kinetic energy and this increases with Wi_3.

The axial velocity profile and the contours of the stream function perturbation for this case are plotted in Figs. 10 and 11. Here the maximum of the axial velocity perturbation occurs close to the bottom gel-liquid interface as the bottom fluid has a lower viscosity. This suggests that the instability arises due to the stress generated by the no-slip condition at the walls. In Fig. 11 the streamline contours are denser near the bottom gel-liquid interface. The gradient of the stream function along the y direction increases as we approach the bottom gel-liquid interface, as the velocity is at maximum here.

Typical neutral stability curves in the Wi_3-k plane for the LL short-wave instability are shown in Fig. 12. These curves have a minimum at a finite wave number, which corresponds to the critical value of Wi_3. Perturbations with the corresponding wave number become unstable when Wi_3 is increased beyond this critical value. For a fixed wave number, as the viscosity ratio μ_{21} increases from 0.1 to 0.15, the critical Weissenberg number Wi_3 required for the flow to become unstable increases. For an increase in the viscosity ratio μ_{21} the critical Weissenberg number occurs for higher wave numbers. An increase in the viscosity ratio μ_{21} results in an increase in viscous dissipation in fluid 2. Consequently a higher Wi_3 is required to generate sufficient Reynolds stresses to destabilize the flow.

Critical surfaces in the $\mathrm{Wi}_3-\mathrm{Re}_1$ plane across which stability changes are shown in Fig. 13. The critical Reynolds number required for this instability for a given Wi_3 can be obtained from this figure. For a fixed Reynolds number as the viscosity ratio μ_{21} increases from 0.1 to 0.2 the Weissenberg number required for this instability to set in increases. Consequently for this mode to evolve the flexibility of the soft-gel layers has to be increased when we increase viscosity ratio μ_{21}. The flexible nature of the wall decreases the Reynolds number required for the onset of instability for a fixed μ_{21}. Similarly the critical Weissenberg number Wi_3 increases as the Reynolds number Re_1 decreases for a fixed viscosity ratio.

F. Destabilization of gel-liquid interfaces

1. *Destabilization for rigid bottom wall gel coating only at top wall*

In this section we focus on the gel-liquid interface which can potentially become unstable under some operating conditions. This is a new instability mode referred to as the GL short-wave mode which cannot be observed in flows between rigid walls. To focus on this mode, we choose the parameters so that the

TABLE I. Contribution of various energy terms obtained from energy analysis for LL short-wave instability shown in Fig. 9(a).

Wi_3/k	$\sum_{j=1}^{2} E_{\mathrm{KE},j}$	$\sum_{j=1}^{2} E_{\mathrm{REY},j}$	$E_{\mathrm{TAN},1}$	$E_{\mathrm{TAN},2}$	$E_{\mathrm{TAN},3}$	$E_{\mathrm{NOR},1}$	$E_{\mathrm{NOR},2}$	$E_{\mathrm{NOR},3}$	$\sum_{j=1}^{4} E_{\mathrm{DIS},j}$
0.05/1.3	0.3072	**0.7149**	0.0379	0	−0.0511	−0.0001	0.0001	0.5971	−1
0.1/1.25	0.5399	**0.9775**	0.0151	0	−0.0524	−0.0003	0.00015	0.5999	−1

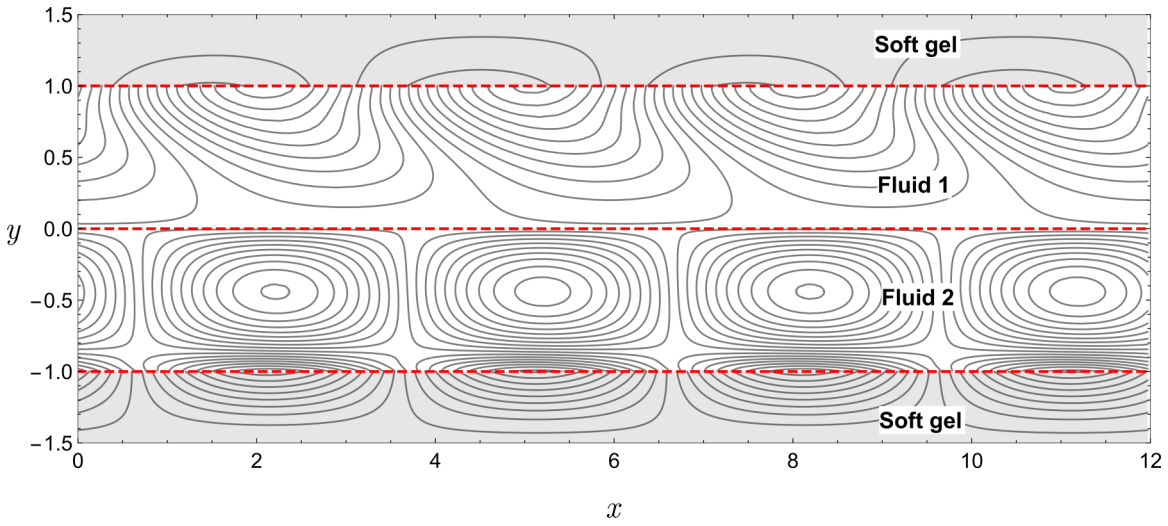

FIG. 11. Contours of stream function perturbation for the LL short-wave instability for $0 \leqslant x \leqslant 2l_{\text{wave}}$ and $-1 \leqslant y \leqslant 1$ where $l_{\text{wave}} = 2\pi/k$. Other parameters are $n_{21} = 1$, $n_{31} = 1.5$, $n_{41} = 1.5$, $\mu_{31} = 10$, $\mu_{41} = 10, \rho_{21} = 1.16$, $\text{Re}_1 = 700$, $S_{31} = S_{41} = 0.0001$, $S_{21} = \frac{829}{\text{Re}_1^2}$, $\mu_{21} = 0.1$, $\text{Wi}_3 = \text{Wi}_4 = 0.2$.

other instability modes are suppressed. We set $\mu_{21} = 1$, to eliminate LL long-wave mode and analyze in the creeping flow limit to eliminate the LL short-wave mode.

We analyze the GL short-wave mode for the top gel-liquid interface alone by setting $\text{Wi}_4 = 0.001$. The dispersion curves for this mode are shown in Fig. 14(a) for low surface tensions of the gel-liquid interface. The energy analysis for the dispersion curves in Fig. 14(a) for different Wi_3 is given in the Supplemental Material [26]. Here the dominant energy term which contributes to the instability is $E_{\text{TAN},2}$, the tangential stress at the top gel-liquid interface where the deformable gel is present. It can be also seen from Fig. 14(a) that when the Weissenberg number Wi_3 is increased from 2 to 5, the GL short-wave mode is destabilized; i.e., the growth rate increases. This destabilization is due to a relative increase in the tangential stresses at the top gel-liquid interface, i.e., $E_{\text{TAN},2}$ in the energy analysis. However, when Wi_3 is further increased from 5 to 15 the growth rate of this mode decreases. This is due to the stabilization effect of the normal stresses $E_{\text{NOR},2}$ at the top gel-liquid interface which becomes negative in the energy budget. In Fig. 14(b) we see that for large surface tension at the gel-liquid interface, the maximum growth rate shifts towards lower wave numbers with an increase in Wi_3.

We plot the perturbed stream lines shown in Fig. 15 for the GL short-wave mode. The gradient of the stream function along the y direction in the top gel layer increases as we approach the top gel-liquid interface. This indicates that the top gel-liquid interface plays a major role in flow destabilization. For the LL short-wave mode, the maximum of the perturbed axial velocity occurs near the wall in the less viscous fluid. In the GL short-wave mode the maximum of the velocity occurs at the gel-liquid interface as shown in Fig. 16.

Critical surfaces in the $\text{Wi}_3 - n_{31}$ plane across which stability changes are shown in Fig. 17. It can be seen that with an increase in the viscosity ratio μ_{31} from 1 to 1.5,

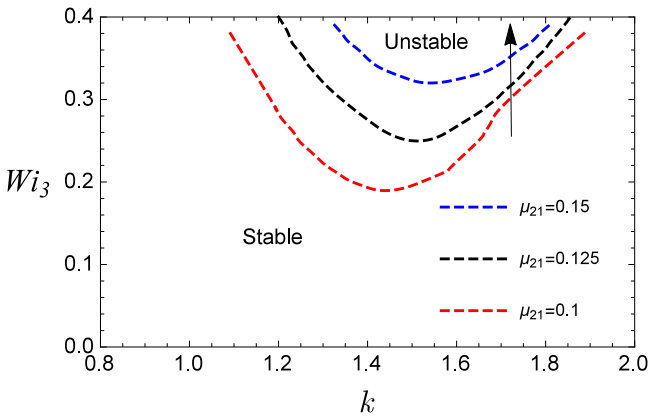

FIG. 12. Effect of μ_{21} on the neutral stability curve for the LL short-wave mode (arrow points in the direction of increasing μ_{21}). Here $\text{Wi}_3 = \text{Wi}_4$. Other parameters: $n_{21} = 1, n_{31} = 1.5, n_{41} = 1.5$, $\mu_{31} = 10, \mu_{41} = 10, \rho_{21} = 1.16, \text{Re}_1 = 230, S_{21} = \frac{829}{\text{Re}_1^2}, S_{31} = S_{41} = 0.0001$.

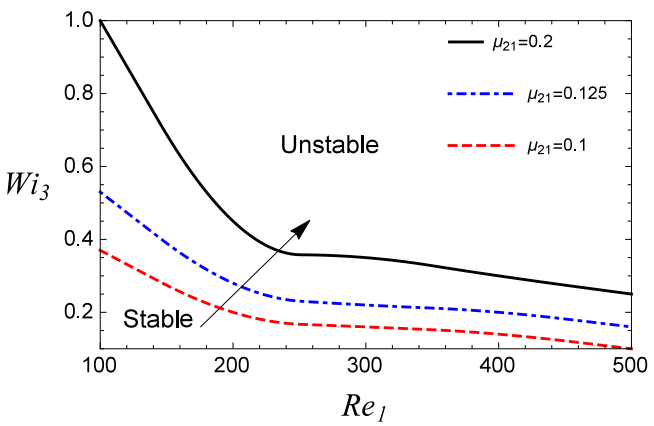

FIG. 13. Effect of μ_{21} on the Wi_3-Re_1 critical surfaces for the LL short-wave mode. Here $\text{Wi}_3 = \text{Wi}_4$. Other parameters are $n_{21} = 1, n_{31} = 1.5, n_{41} = 1.5, \mu_{31} = 10, \mu_{41} = 10, \rho_{21} = 1.16, S_{21} = \frac{829}{\text{Re}_1^2}$, $S_{31} = S_{41} = 0.0001$.

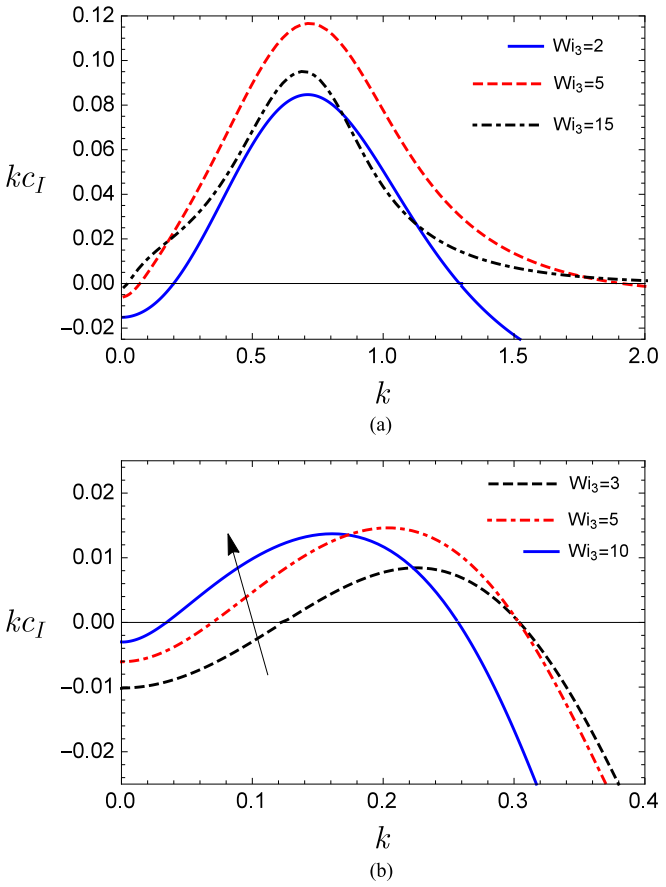

FIG. 14. Dispersion curves for the GL short-wave mode. The arrow points in the direction of the increasing Wi_3. (a) Other parameters: $n_{21}=1$, $n_{31}=4$, $n_{41}=4$, $\mu_{21}=1$, $\mu_{31}=\mu_{41}=1$, $\rho_{21}=1$, $\mathrm{Wi}_4=0.001$, $\mathrm{Re}_1=0.01$, $S_{21}=0$, $S_{31}=S_{41}=0.01$; (b) $n_{21}=1$, $n_{31}=4$, $n_{41}=4$, $\mu_{21}=1$, $\mu_{31}=\mu_{41}=1$, $\rho_{21}=1$, $\mathrm{Wi}_4=0.001$, $\mathrm{Re}_1=1$, $S_{21}=0$, $S_{31}=S_{41}=10$.

the critical Wi_3 required for this instability increases. The evolution of this mode is characterized by the dominance of the tangential stress term $E_{\mathrm{TAN},2}$. For high values of Wi_3, the shear modulus discontinuity across the top gel-liquid interface

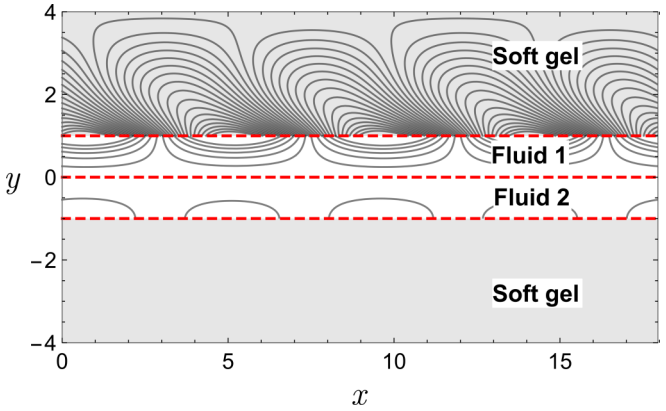

FIG. 15. Contours of stream function perturbation for the GL short-wave instability show in Fig. 14(a) for $0 \leqslant x \leqslant 2l_{\mathrm{wave}}$ and $-1 \leqslant y \leqslant 1$ where $l_{\mathrm{wave}} = 2\pi/k$.

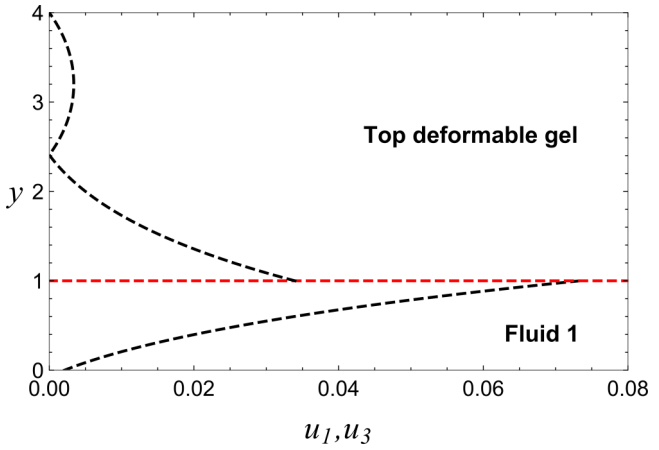

FIG. 16. Perturbed velocity in the top liquid and top gel. Other parameters: $n_{21}=1$, $n_{31}=4$, $n_{41}=4$, $\mu_{21}=1$, $\mu_{31}=\mu_{41}=1$, $\rho_{21}=1$, $\mathrm{Wi}_4=0.001$, $\mathrm{Re}_1=0.01$, $S_{21}=0$, $S_{31}=S_{41}=0.01$.

is significant. This creates dominant tangential stresses at this gel-liquid interface, which overcomes the stabilization caused by the viscous dissipation in the soft-gel layer. For a given Wi_3 this mode can be suppressed by choosing a sufficiently low thickness of the top gel layer.

2. *Destabilization of both top and bottom gel-liquid interfaces*

We now discuss the case when both the top and bottom walls are coated by a gel and $\mathrm{Wi}_3=10$, $\mathrm{Wi}_4=5$. The corresponding dispersion curves are shown in Fig. 18. From the energy analysis (see Supplemental Material [26]) we see that the dominant destabilizing contributions where the two maxima occur come from the $E_{\mathrm{TAN},2}$ and $E_{\mathrm{TAN},3}$ terms, i.e., the tangential stresses at the top and bottom gel-liquid interfaces. The first peak in the dispersion curve at $k=0.2$ implies that the $E_{\mathrm{TAN},2}$ term gives the major destabilization contribution to the energy budget. This is the contribution from the increased flexible nature of the top gel-liquid interface. The second peak

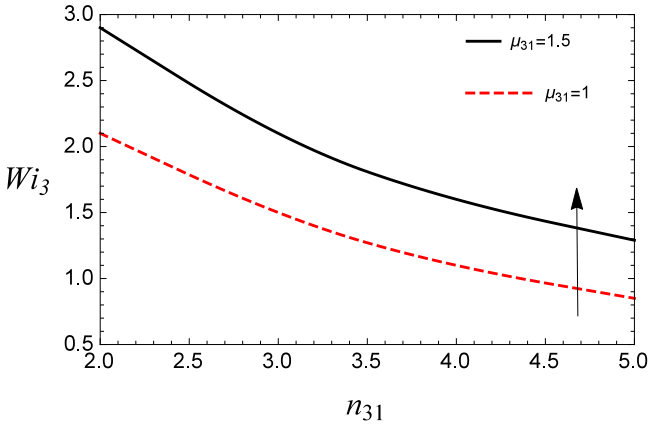

FIG. 17. Effect of μ_{31} on the critical surface in the Wi_3 - n_{31} plane for the GL short-wave mode instability. Other parameters: $n_{21}=1$, $\mu_{21}=1$, $\rho_{21}=1$, $\mathrm{Re}_1=0$, $S_{21}=0.0001$, $S_{31}=S_{41}=0$, $\mathrm{Wi}_4=0.001$. Arrow points in the direction of increase in the viscosity ratio μ_{31}.

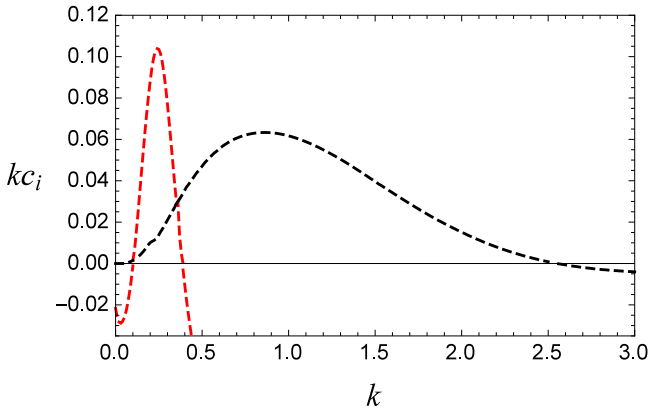

FIG. 18. Dispersion curve when both the top and bottom GL short-wave modes of instabilities coexist in the flow (the arrow points in the direction of increasing Wi_4). Other parameters: $n_{21} = 1, n_{31} = 6, n_{41} = 6,\ \mu_{21} = 1, \mu_{31} = \mu_{41} = 1,\ \rho_{21} = 1,\ S_{21} = 10^{-5}$, $S_{31} = S_{41} = 10$, $\mathrm{Re}_1 = 10^{-3}$, $\mathrm{Wi}_3 = 10$, and $\mathrm{Wi}_4 = 5$.

in this dispersion curve which occurs for $k = 0.9$ corresponds to the dominance of the $E_{\mathrm{TAN},3}$ term in the energy budget. For the gel-liquid interface with higher (lower) Weissenberg number the maximum growth rate occurs for lower (higher) wave numbers. This is to be expected since when the surface tension is high at the gel-liquid interface the wave number corresponding to the maximum growth rate decreases as Wi_3 increases [see Fig. 14(b)].

Figure 19 shows the 2D contours of the stream function perturbation when both the top and bottom walls have a gel coating. We observe two vortices in the stream function contour plot. One vortex is close to the top gel-liquid interface and the other close to the bottom gel-liquid interface, confirming that both gel-liquid interfaces play a major role in the destabilization of the base state.

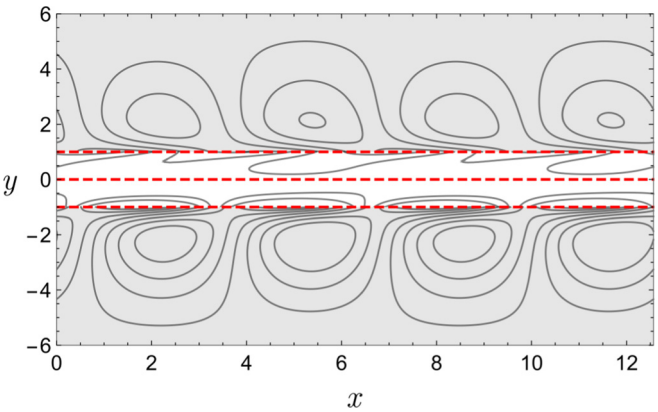

FIG. 19. Contours of stream function perturbation for the GL instability for $0 \leqslant x \leqslant 2l_{\mathrm{wave}}$ and $-1 \leqslant y \leqslant 1$ where $l_{\mathrm{wave}} = 2\pi/k$. Other parameters: $n_{21} = 1, n_{31} = 6, n_{41} = 6, \mu_{21} = 1, \mu_{31} = \mu_{41} = 1, \rho_{21} = 1, S_{21} = 10^{-5}, \rho_{31} = \rho_{41} = 1, S_{31} = S_{41} = 10\ \mathrm{Re}_1 = 10^{-3}$, $\mathrm{Wi}_3 = 10$, and $\mathrm{Wi}_4 = 5$.

VII. CONCLUSIONS

In this paper our study focuses on the linear stability of layered two-phase flow through a channel whose walls are coated by a soft gel. The soft-gel layers play a significant role in influencing the stability characteristics of the flow. By analyzing systematically the energy contributions of various processes in the perturbed flow, insights into the physical mechanism driving the different instabilities are obtained.

We first analyzed the flow configuration using a long-wave asymptotic analysis. This was used to validate the numerical solution of the general linearized problem. In the absence of the soft-gel layers, the liquid-liquid interface exhibits a long-wave instability arising from the viscosity difference across the interface. The asymptotic analysis shows that the effect of the soft-gel layer influences the growth rate at $O(k)$. The deformable nature of the soft-gel layers can have either a stabilizing or a destabilizing effect on the LL long-wave mode. The μ_{21}-n_{21} parameter space is divided into four regions. The stability characteristics of the interfacial LL long-wave mode are dictated by the arrangement of the fluids in the two-phase layered flow. In region 1 and region 3, where a more viscous fluid is placed near a gel layer, the corresponding gel layer has a dominant stabilizing effect on the LL long-wave mode. An unexpected result is that in region 2 and region 4, a gel layer placed near a less viscous and narrow fluid has a dominant destabilizing effect on the LL long-wave mode. The presence of the gel layers can render regions 1 and 3 stable and regions 2 and 4 unstable in Fig. 4(b). Energy analysis shows that the LL long-wave mode is primarily induced by viscosity difference across the liquid-liquid interface. This is confirmed by the dominant $E_{\mathrm{TAN},1}$ term in the energy analysis. Stabilization of the LL long-wave mode is explained by the decrease in the magnitude of the $E_{\mathrm{TAN},1}$ term relative to viscous dissipation in the energy analysis with increase in Wi_3. The destabilization of the LL long-wave mode is characterized by the tangential stresses created at the gel-liquid interfaces, i.e., the $E_{\mathrm{TAN},2}$ and $E_{\mathrm{TAN},3}$ terms in the energy analysis.

The presence of soft-gel layers at the walls destabilizes the LL short-wave instability which is governed by shear stresses. This is confirmed by the dominance of the $\sum_{j=1}^{2} E_{\mathrm{REY},j}$ term in the energy analysis. An important result of this work is that new instabilities arise in the flow due to the deformable nature of the soft-gel layers. From numerical computations it is shown that a GL short-wave instability mode can arise in the system even when the other modes are absent. This is caused by the differences in the shear modulus across the gel-liquid interface. The GL short-wave instability arises due to the dominance of the $E_{\mathrm{TAN},2}$ and $E_{\mathrm{TAN},3}$ terms in the energy analysis.

The GL short-wave instability originates at the gel-liquid interface only when the gel thickness and deformability are well above their critical values. This instability mode is also characterized by two peaks in the dispersion curves when both walls have a soft-gel layer coating.

The stabilization (destabilization) of the LL long-wave mode due the deformable soft-gel layers is observed for Weissenberg number $\mathrm{Wi}_3 = \mathrm{Wi}_4 = 0.05$ ($\mathrm{Wi}_3 = \mathrm{Wi}_4 = 5$) and moderate Reynolds numbers $\mathrm{Re}_1 < 30$. On the other hand

the destabilization of the LL short-wave mode due to the soft-gel layers is observed for $\mathrm{Wi}_3 = \mathrm{Wi}_4 < 0.25$ and large Re_1; i.e., $\mathrm{Re}_1 > 100$. For $2 < \mathrm{Wi}_3 = \mathrm{Wi}_4 < 15$ and $0.001 < \mathrm{Re}_1 < 1$ the GL short-wave mode at the gel-liquid interface evolves. The GL short-wave mode is observed only for large Weissenberg numbers as compared to the LL long-wave and LL short-wave modes.

To physically understand the evolution of different instabilities, equidensity contour plots of the stream functions are plotted. In the case of the LL long-wave mode the density of the contours is high at the liquid-liquid interface providing additional evidence that the LL long-wave mode evolves along the liquid-liquid interface. For LL short-wave instability the density of the stream function is high near the gel-liquid interface in the less viscous fluid. For the GL short-wave instability the density of the contour plots is high in the top and bottom gel layers. This implies that the GL short-wave instability arises due to the deformable nature of the both gel layers. These plots hence provide insight into the cause of the dominant physical effect for an instability.

In summary, introducing a deformable soft-gel layer along rigid walls helps in controlling and manipulating different instabilities in multilayer flows. An important task for future work is to extend the current two-dimensional analysis to three-dimensional geometries taking into account the dependency of the perturbation in the z direction [34,35]. In an effort to understand different instabilities in the flow configuration we have used a linear viscoelastic model for the soft-gel layers. The stability characteristics of the flow configuration would change if we were to use a different model such as a neo-Hookean model for the soft-gel layers [18].

APPENDIX: LONG-WAVE ANALYSIS FOR LAYERED FLOW THROUGH GEL-COATED WALLS

1. Leading order analysis

The governing equations for the leading order velocity fields in the fluids and the leading order displacement fields in the soft-gel layers obtained from the asymptotic series expansion are

$$d_y^4 v_j^{(0)} = 0. \tag{A1}$$

From continuity equation (17) the governing equation for the axial velocity fields in the fluids is

$$u_j^{(0)} = i d_y v_j^{(0)}.$$

From the x momentum Eq. (18) the governing equation for the pressure in the fluids is

$$p_j^{(0)} = \frac{-i\mu_{j1}}{\mathrm{Re}_1} d_y^2 u_j^{(0)}. \tag{A2}$$

The governing equation for the leading order displacement field in the y direction for the soft gels is

$$d_y^4 Y_j^{(0)} = 0. \tag{A3}$$

The governing equation for the leading order displacement field in the x direction for the soft gels is

$$X_j^{(0)} = i d_y v_j^{(0)}. \tag{A4}$$

The governing equation for the leading order pressure in the soft gels is

$$p_j^{(0)} = \frac{-i\mu_{j1}}{\mathrm{Re}_1 \mathrm{Wi}_j} d_y^2 u_j^{(0)}. \tag{A5}$$

At the liquid-liquid interface at $y = 0$, the following boundary conditions at the leading order are imposed.

Continuity of axial component of velocity:

$$\left(u_1^{(0)} - u_2^{(0)}\right)(U_0 - c^{(0)}) - \left[i v_1^{(0)}(d_y U_1 - d_y U_2)\right] = 0. \tag{A6}$$

Continuity of vertical component of velocity:

$$v_1^{(0)} - v_2^{(0)} = 0. \tag{A7}$$

Tangential stress condition at the liquid-liquid interface:

$$d_y u_1^{(0)} - \mu_{21} d_y u_2^{(0)} = 0. \tag{A8}$$

Normal stress condition at the liquid-liquid interface:

$$\mathrm{Re}_1\left(p_2^{(0)} - p_1^{(0)}\right)(U_1 - c^{(0)}). \tag{A9}$$

The leading order boundary conditions at the top gel-liquid interface at $y = 1$ are as follows.

Continuity of velocity in the axial direction:

$$u_1^{(0)} = 0. \tag{A10}$$

Continuity of velocity in the y direction:

$$v_1^{(0)} = 0. \tag{A11}$$

Tangential stress condition at the top gel-liquid interface:

$$d_y u_1^{(0)} - \frac{\mu_{31}}{\mathrm{Wi}_3} d_y X_3^{(0)} = 0. \tag{A12}$$

Normal stress condition at the top gel-liquid interface:

$$\mathrm{Re}_1\left(p_1^{(0)} - p_3^{(0)}\right) = 0. \tag{A13}$$

The leading order boundary conditions at the bottom gel-liquid interface at $y = -n_{21}$ are as follows.

Continuity of axial component of velocity:

$$u_2^{(0)} = 0. \tag{A14}$$

Continuity of velocity in the y direction:

$$v_2^{(0)} = 0. \tag{A15}$$

Tangential stress condition at the bottom gel-liquid interface:

$$d_y u_2^{(0)} - \frac{\mu_{41}}{\mathrm{Wi}_4} d_y X_4^{(0)} = 0. \tag{A16}$$

Normal stress condition at the bottom gel-liquid interface:

$$\mathrm{Re}_1\left(p_4^{(0)} - p_2^{(0)}\right) = 0. \tag{A17}$$

Leading order boundary conditions at the rigid surfaces at $y = n_{31}$ and $y = -n_{41}$:

$$u_3^{(0)} = 0, \quad v_3^{(0)} = 0, \tag{A18}$$

$$u_4^{(0)} = 0, \quad v_4^{(0)} = 0. \tag{A19}$$

The leading order equation (A1) for $v_1^{(0)}$ and $v_2^{(0)}$ are integrated to obtain

$$v_1^{(0)} = A_1 y^3 + A_2 y^2 + A_3 y + A_4, \tag{A20}$$

$$v_2^{(0)} = B_1 y^3 + B_2 y^2 + B_3 y + B_4. \tag{A21}$$

The leading order equations (A3) for $Y_3^{(0)}$ and $Y_4^{(0)}$ are integrated to obtain

$$Y_1^{(0)} = D_1 y^3 + D_2 y^2 + D_3 y + D_4, \tag{A22}$$

$$Y_2^{(0)} = E_1 y^3 + E_2 y^2 + E_3 y + E_4. \tag{A23}$$

Equations (A1)–(A23) are solved along with the boundary conditions at the leading order to obtain the coefficients A_i, B_i, D_i, and E_i (where $i = 1, \ldots, 4$) to determine the leading order growth rate. At the leading order the fluid velocities satisfy the no-slip boundary condition at the gel-liquid interfaces. At the leading order, the presence of the soft gel does not contribute to the continuity of fluid velocities at the gel-liquid interfaces. This implies that the effect of the deformability of the gel layers does not influence the leading order velocities. Hence, the leading order wave speed is identical to the expression in [27]. The leading order velocity in the fluids generates stress on the gel layers through the tangential stress boundary condition. This stress generates deformation in the gel layers at the leading order.

2. First correction

The governing equations for the velocity fields in the fluids and the displacement fields in the soft gels at the first order in asymptotic analysis are now described.

The governing equation for the fluid velocities in the y direction at first order is

$$d_y^4 v_j^{(1)} = \frac{i\mathrm{Re}_1 \rho_{j1}}{\mu_{j1}} \left\{ \left[(U_0 - c^{(0)}) d_y^2 v_j^{(0)} \right] - d_y^2 U_j v_j^{(0)} \right\}. \tag{A24}$$

The governing equation for fluid velocities in the axial direction is

$$u_j^{(1)} = i d_y v_j^{(1)}. \tag{A25}$$

The governing equation for the pressure in the fluids is

$$p_j^{(1)} = i \left[\left(\frac{-\mu_{j1}}{\mathrm{Re}_1 \rho_{j1}} d_y^2 u_j^{(1)} \right) + \left(-i c^{(0)} u_j^{(0)} \right) + \left(i U_j u_j^{(0)} \right) + d_y U_j v_j^{(0)} \right]. \tag{A26}$$

Boundary conditions at the liquid-liquid interface at the first order are as follows.

Continuity of velocity in the flow direction:

$$k\left[c^{(1)} \left(u_2^{(1)} - u_1^{(1)} \right) + U_1 \left(u_1^{(1)} - u_2^{(1)} \right) + c^{(0)} \left(u_2^{(1)} - u_1^{(1)} \right) - i v_1^{(1)} (d_y U_1 - d_y U_2) \right] = 0. \tag{A27}$$

Continuity of velocity in the y direction:

$$k \left(v_1^{(1)} - v_2^{(1)} \right) = 0. \tag{A28}$$

Tangential stress condition at the liquid-liquid interface:

$$d_y u_1^{(1)} - \mu_{21} d_y u_2^{(1)} = 0. \tag{A29}$$

Normal stress condition at the liquid-liquid interface:

$$k\mathrm{Re}_1 \left[c^{(1)} \left(p_2^{(0)} - p_1^{(0)} \right) + U_1 \left(p_1^{(1)} - p_2^{(1)} \right) + c^{(0)} \left(p_2^{(1)} - p_1^{(1)} \right) \right] = 0. \tag{A30}$$

Boundary conditions at the top gel-liquid interface at the first order are as follows.

Continuity of velocity in the axial direction:

$$k\left[u_1^{(1)} + \left(d_y U_1 v_3^{(0)} \right) + \left(i c^{(0)} u_3^{(0)} \right) \right] = 0. \tag{A31}$$

Continuity of velocity in the y direction:

$$k\left[v_1^{(1)} + \left(i c^{(0)} v_3^{(0)} \right) \right] = 0. \tag{A32}$$

Tangential stress condition at the top gel-liquid interface:

$$k\left[d_y u_1^{(1)} + \mu_{31} i c^{(0)} d_y u_3^{(0)} \right] = 0. \tag{A33}$$

Normal stress condition at the top gel-liquid interface:

$$k\mathrm{Re}_1 p_1^{(1)} = 0. \tag{A34}$$

Boundary conditions at the bottom gel-liquid interface are as follows.

Continuity of velocity in the axial direction:

$$k\left[u_2^{(1)} + \left(d_y U_2 v_4^{(0)} \right) + \left(i c^{(0)} u_4^{(0)} \right) \right] = 0. \tag{A35}$$

Continuity of velocity in the y direction:

$$k\left[v_2^{(1)} + \left(i c^{(0)} v_4^{(0)} \right) \right] = 0. \tag{A36}$$

Tangential stress condition at the top gel-liquid interface:

$$k\left[d_y u_2^{(1)} + \frac{\mu_{41}}{\mu_{21}} i c^{(0)} d_y u_4^{(0)} \right] = 0. \tag{A37}$$

Normal stress condition at the top gel-liquid interface:

$$k\mathrm{Re}_1 p_2^{(1)} = 0. \tag{A38}$$

Equations (A24)–(A38) are solved to determine the growth rate at the first order.

[1] T. M. Squires and S. R. Quake, Rev. Mod. Phys. **77**, 977 (2005).

[2] M. A. Unger, H. P. Chou, T. Thorsen, A. Scherer, and S. R. Quake, Science **288**, 113 (2000).

[3] H. A. Stone, A. D. Stroock, and A. Ajdari, Annu. Rev. Fluid Mech. **36**, 381 (2004).

[4] P. A. M. Boomkamp and R. H. M. Miesen, Int. J. Multiphase Flow **22**, 67 (1996).

[5] C.-S. Yih, J. Fluid Mech. **27**, 337 (1967).

[6] S. G. Yiantsios and B. G. Higgins, J. Comput. Phys. **2540**, 16 (1988).

[7] B. S. Tilley, S. H. Davis, and S. G. Bankoff, Phys. Fluids **6**, 3906 (1994).
[8] R. Govindarajan and K. C. Sahu, Annu. Rev. Fluid Mech. **46**, 331 (2014).
[9] T. J. O. Hern, J. Fluid Mech. **215**, 365 (1990).
[10] N. Andritsos, L. Williams, and T. J. Hanratty, Int. J. Multiphase Flow **15**, 877 (1989).
[11] C. Tzotzi and N. Andritsos, Int. J. Multiphase Flow **54**, 43 (2013).
[12] M. Birvalski, M. J. Tummers, R. Delfos, and R. A. W. M. Henkes, Int. J. Multiphase Flow **62**, 161 (2014).
[13] V. Kumaran, G. H. Fredrickson, and P. Pincus, J. Phys. II **4**, 893 (1994).
[14] V. Kumaran, J. Fluid Mech. **294**, 259 (1995).
[15] V. Kumaran, J. Fluid Mech. **357**, 123 (1998).
[16] V. Kumaran, J. Fluid Mech. **362**, 1 (1998).
[17] V. Kumaran, Curr. Sci. **79**, 766 (2000).
[18] V. Gkanis and S. Kumar, Phys. Fluids **15**, 2864 (2003).
[19] V. Gkanis and S. Kumar, J. Fluid Mech. **524**, 357 (2005).
[20] V. Gkanis and S. Kumar, Phys. Fluids **18**, 044103 (2006).
[21] V. Shankar, J. Non-Newtonian Fluid Mech. **117**, 163 (2004).
[22] P. Chokshi and V. Kumaran, Phys. Rev. E **77**, 056303 (2008).
[23] V. Shankar and L. Kumar, Phys. Fluids **16**, 4426 (2004).
[24] Gaurav and V. Shankar, Phys. Fluids **22**, 094103 (2010).
[25] Gaurav and V. Shankar, Phys. Fluids **25**, 014104 (2013).
[26] See Supplemental Material at http://link.aps.org/supplemental/10.1103/PhysRevE.96.013119 for energy budget analysis for different regions of the stability map and GL instability modes.
[27] S. G. Yiantsios and B. G. Higgins, Phys. Fluids **31**, 3225 (1988).
[28] L. G. Leal, *Advanced Transport Phenomena*, 1st ed. (Cambridge University Press, New York, 2007).
[29] J. R. Picardo, T. G. Radhakrishna, and S. Pushpavanam, J. Fluid Mech. **793**, 280 (2016).
[30] P. A. M. Boomkamp, B. J. Boersma, R. H. M. Miesen, and G. V. Beijnon, J. Comput. Phys. **132**, 191 (1997).
[31] J. P. Boyd, *Chebyshev and Fourier Spectral Methods*, 2nd ed. (Dover, New York, 2001).
[32] T. A. Canuto, C. Hussaini, M. Y. Quarteroni, and A. Zang, *Spectral Methods: Evolution to Complex Geometries and Applications to Fluid Dynamics*, 1st ed. (Springer-Verlag, Berlin, Heidelberg, 2007).
[33] I. Barmak, A. Gelfgat, H. Vitoshkin, A. Ullmann, and N. Brauner, Phys. Fluids **28**, 044101 (2016).
[34] K. C. Sahu and O. K. Matar, Phys. Fluids **22**, 112103 (2010).
[35] M. H. Allouche, S. Millet, V. Botton, D. Henry, H. Ben Hadid, and F. Rousset, Phys. Rev. E. **92**, 063010 (2015).